CHAPTER 116

Numerical simulation of nonlinear wave interacting with permeable breakwaters

T.Sakakiyama[1] and R.Kajima[2]

Abstract

A fully nonlinear simulation model was developed to predict the wave transformation interacting with a permeable breakwater. The present model was applied to simulate wave transformations due to a rubble-mound breakwater and due to a caisson breakwater covered with armor units and verified by hydraulic model tests. Numerical experiments were also performed to interpret the stability of armor units and the wave-induced pressure on the caisson through the pile of armor units.

1. INTRODUCTION

Numerical models to predict wave motions near and inside of a rubble mound breakwater have been recently developed. Since some models are based on the linear wave theory (Hölscher *et al.*, 1989), they provide only a change of amplitude of a sinusoidal wave. Others are nonlinear but one-dimensional models, *i.e.*, they are based on the depth-integrated equations (Wurjanto and Kobayashi,1992). Ohyama and Nadaoka(1991) developed a fully nonlinear model to simulate wave transformation on an impermeable bottom based on the potential theory. No fully nonlinear model including the effect of peremeablity is developed yet.

The purpose of this paper is to develop a fully nonlinear two-dimensional numerical model to predict the wave transformation in the field which is partially occupied by a permeable structure. The interaction between waves and structures is expressed by the resistance forces in the structures, the drag and inertia forces. In this paper, analyzed are the wave transformations due to a rubble-mound breakwater and due to a caisson breakwater covered with armor units both in

[1] Senior research engineer, Central Research Institute of Electric Power Industry, 1646, Abiko, Abiko-city, Chiba, 270-11, Japan.

[2] Senior research fellow, ditto.

front and at back. The computations are compared with hydraulic experimental results. Numerical experiments are also carried out to investigate the wave force acting on the armor units and the wave-induced pressure on the caisson through the pile of armor units.

2. Numerical simulation method

2.1 Governing equation

Sha *et al.*(1977) derived the quasi-continuum governing equations for conservation of mass, momentum and energy called the porous body model(PBM). Their purpose was to apply these equations to the flow in a class of systems, such as heat exchangers and fuel-rod bundles in a nuclear reactor.

The governing equations of PBM for incompressible two-dimensional flow are modified to apply it to the wave field(Sakakiyama,1991). The inertia and the drag forces are introduced into the horizontal and vertical components of the momentum equations, and rearranging them yields the following equations:

Continuity equation

$$\frac{\partial(\gamma_x u)}{\partial x} + \frac{\partial(\gamma_z w)}{\partial z} = 0, \tag{1}$$

Momentum equation

$$\lambda_v \frac{\partial u}{\partial t} + \lambda_x u \frac{\partial u}{\partial x} + \lambda_z w \frac{\partial u}{\partial z} = -\gamma_v \frac{\partial \phi}{\partial x} - R_x + \frac{1}{\rho}\left\{\frac{\partial(\gamma_x \tau_{xx})}{\partial x} + \frac{\partial(\gamma_z \tau_{zx})}{\partial z}\right\}, \tag{2}$$

$$\lambda_v \frac{\partial w}{\partial t} + \lambda_x u \frac{\partial w}{\partial x} + \lambda_z w \frac{\partial w}{\partial z} = -\gamma_v \frac{\partial \phi}{\partial z} - \gamma_v g - R_z + \frac{1}{\rho}\left\{\frac{\partial(\gamma_x \tau_{xz})}{\partial x} + \frac{\partial(\gamma_z \tau_{zz})}{\partial z}\right\}, \tag{3}$$

where

$$\left.\begin{aligned} \lambda_v &= \gamma_v + (1-\gamma_v)C_M \\ \lambda_x &= \gamma_x + (1-\gamma_v)C_M \\ \lambda_z &= \gamma_z + (1-\gamma_v)C_M \end{aligned}\right\} \tag{4}$$

and λ_v is the volume porosity and λ_x, λ_z the horizontal and vertical components of the surface permeabilty, respectively. $\phi = p/\rho$ is the ratio of the pressure p to the density of the fluid ρ and u, w the velocity components in the x- and z-direction respectively, g the acceleration due to gravity, τ the viscous stress acting on the surface of the control volume. The drag forces are modeled by Eq. (5) and Eq. (6),

$$R_x = \frac{C_D}{2\Delta x}(1-\gamma_x)u\sqrt{u^2+w^2} \tag{5}$$

$$R_z = \frac{C_D}{2\Delta z}(1-\gamma_z)w\sqrt{u^2+w^2} \tag{6}$$

Unknown are the inertia and drag coefficients C_M, C_D, which are experimentally determined.

2.2 Boundary conditions

The continuity equation Eq. (1) and the momentum equations (2) and (3) are numerically solved with appropriate boundary and initial conditions.

A kinematic boundary condition on the free surface is expressed as:

$$\frac{\partial \eta}{\partial t} + u_S \frac{\partial \eta}{\partial x} = w_S \tag{7}$$

where η is the free surface displacement, u_S and w_S are the horizontal and vertical components of the velocity on the free surface η, respectively.

A dynamic boundary condition at the free surface is represented by the following:

$$p = 0 \qquad \text{on} \quad z = \eta \tag{8}$$

At a bottom boundary, a free slip condition is imposed. When a water depth is uniform, the slip conditions for the velocity u, w and the pressure p are expressed as follows:

$$\frac{\partial u}{\partial z} = 0 \tag{9}$$

$$w = 0 \tag{10}$$

$$\frac{\partial p}{\partial z} = -\rho g \tag{11}$$

The boundary condition on the pressure given by Eq. (11) is led by substituting Eq. (10) into the vertical component of the momentum equation, Eq. (3). In the case that a boundary contains an impermeable vertical wall, the similar free slip condition is imposed at the impermeable boundary.

An inflow boundary works as a wavemaker. Perturbation solutions of the nonlinear wave theory by Isobe *et al.*(1978) are used to give the inflow boundary conditions. The nonlinear wave theory applied to the inflow boundary condition depends on the following wave condition:

$$\left.\begin{array}{lrl} \text{Stokes wave 5th-order solution} & & U_S \leq 25 \\ \text{cnoidal wave 3rd-order solution} & 25 < & U_S \end{array}\right\} \tag{12}$$

where U_S is the shallow water Ursell parameter defined with the long wave length $L = T\sqrt{gh}$ in the Ursell parameter $U_r = HL^2h^3$;

$$U_S = \frac{gHT^2}{h^2}. \tag{13}$$

At an outflow boundary, Sommerfeld's radiation condition is imposed:

$$\frac{\partial F}{\partial t} + C\frac{\partial F}{\partial x} = 0 \tag{14}$$

where C is the wave celerity and F denotes the variable η, u, w or p. Eq. (14) indicates that the variable F progresses with the phase speed C.

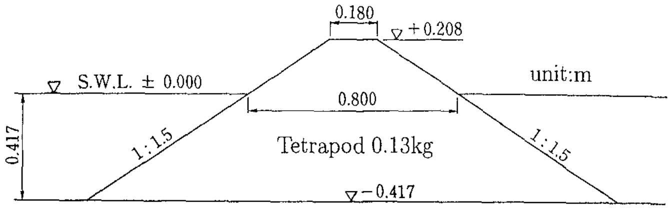

Fig. 1 Rubble-mound breakwater($\lambda = 1/60$)

Table 1 Experimental conditions for rubble-mound breakwater(λ=1/60)

wave period	wave height	water depth	Tetrapod		
T(s)	H(m)	h(m)	W(kg)	b(m)	ε
1.50	0.015–0.275	0.417	0.13	0.059	0.53

The initial condition is set as the still water state. The surface displacement η at $t = 0$ is null for a whole computational region as well as $u = w = 0$. The pressure p at $t = 0$ is given by the hydrostatic pressure.

The Poisson equation for the pressure is iteratively solved by the successive over-relaxation(SOR) method with the given boundary and initial conditions mentioned above. The dynamic boundary condition on the free surface given by Eq. (8) is exactly satisfied in an iterative process of the pressure computation by applying the "irregular star" method(Chan and Street,1970).

3. Rubble-mound breakwater

3.1 Experiments

The experiments were performed by using a laboratory wave flume (78m long, 1.2m high and 0.9m wide). The model breakwater was a conventional trapezoidal rubble-mound breakwater as shown in Fig. 1. The rubble-mound breakwater consists of single size of Tetrapods(weight W = 0.13kg) for the simplicity to analyze experimental results. The *In Situ* porosity of the breakwater is $\varepsilon = 0.53$. Slopes of the breakwater surface are 1 on 1.5 for both the seaward and landward side surfaces. Table 1 shows the experimental conditions. The model scale is supposed as $\lambda = 1/60$. Water depth at the breakwater is = 0.417m in the model scale and uniform depth h = 0.737m. Wave period was T = 1.5s. Wave height ranges from H = 0.015m to 0.275m. The maximum ratio of the wave height to the water depth H/h was up to about 0.65. The nonlinearity of the waves generated was remarkable but wave breaking was not included in the present experimental conditions.

The reflection coefficient was estimated with the method for resolving incident and reflected waves proposed by Goda(1985). The displacements of a transmitted wave were measured at five locations. The averaged values of the five transmitted wave heights are used in the following analysis.

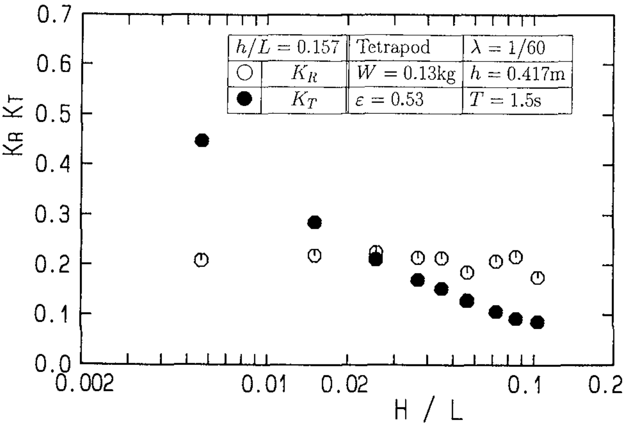

Fig. 2 Reflection and transmission coefficients of rubble-mound breakwater

Table 2 Calculation condition for rubble-mound breakwater

H(m)	T(s)	h(m)	L_I(m)	$\Delta x/L_I$	$\Delta z/h$	$\Delta t/T$	cal. region
0.15	1.5	0.417	3.20	1/71.1	1/13.89	1/200	$8.63 \times L_I$

In Fig. 2, the experimental results of the reflection coefficient K_R and the transmission coefficient K_T are shown as a function of the wave steepness H/L, where L is the wave length at the breakwater($h = 0.417$m) estimated by the linear wave theory. As the wave steepness H/L increases, the transmission coefficient K_T decreases remarkably but the reflection coefficient K_R is almost constant. Basically, the wave reflection depends on the porosity and slightly on the inertial resistance. The wave transmission depends on the energy dissipation in the permeable structure. An amount of the energy dissipation is proportional to the product of the friction factor and the velocity squared.

3.2 Simulation of wave transformation

The computation was carried out under the wave condition as shown in Table 2. The wave period is $T = 1.5$s and the progressive wave height at the breakwater $H = 0.15$m($H/h = 0.36$). The horizontal distance of the calculation region was $8.63 \times L_I$, where L_I is the incident wave length at the uniform depth($h_I = 0.747$m) obtained from the nonlinear wave theory. The wave lengths are $L_I = 3.20$m at the uniform depth and $L = 2.68$m at the breakwater. The space increments are $\Delta x = 0.045$m($\Delta x/L_I = 1/71.1$ and $\Delta x/L = 1/58.9$) horizontally and $\Delta z = 0.03$m($\Delta z/h = 1/13.89$) vertically. The time increment is $\Delta t = T/200$. It took about one hundred minutes with the main frame computer HITAC 680H to calculate 4000 time steps(20 cycles $\times$ 200 steps per wave period) to reach steady state wave motion near the rubble-mound breakwater.

The inertia coefficient C_M and the drag coefficient C_D were estimated so that

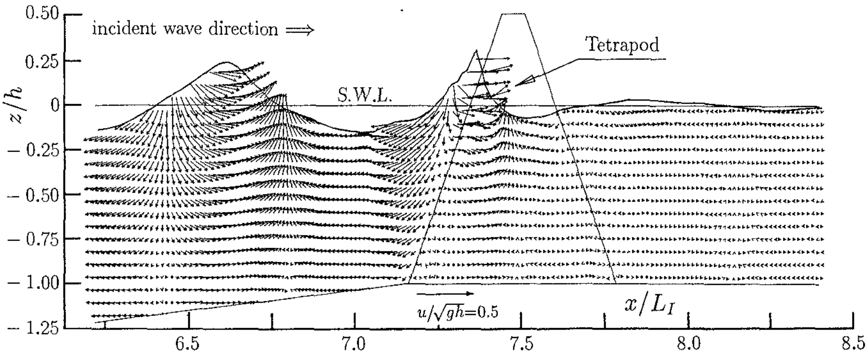

Fig. 3 Simulated result of wave transformation due to rubble-mound breakwater

the reflection and transmission coefficients obtained in the computation might agree well with those in the experiment, respectively. The reflection and transmission coefficients obtained in the computation are $K_R = 0.15$ and $K_T = 0.14$. The corresponding experimental results are $K_R = 0.18$ and $K_T = 0.14$, respectively. The values of $C_D = 1.2$ and $C_M = 1.7$ are obtained by best fitting the computation to the experimental result.

Fig. 3 shows one of the computed wave velocity fields near and within the rubble-mound breakwater. Although a partial standing wave is formed at the windward side of the breakwater, the wave profile and its velocity field are rather similar to those of a progressive wave. It is because of a small reflection coefficient ($K_R = 0.15$ in the computation). Comparing with the profile of partial standing wave, that of wave run-up on the breakwater slope is deformed and becomes steep. The wave attenuation in the permeable breakwater and the wave propagation through it are reasonably simulated.

3.3 Wave force acting on armor units

One of the most important physical phenomenon to investigate the stability of armor units is the movement of wave run-up on a breakwater slope. However, it is quite difficult to measure the velocity and acceleration along the slope during the wave run-up and -down in a hydraulic experiment. Numerical simulation is one of the most useful tools to investigate the wave run-up cooperating with hydraulic experiments. A well-calibrated numerical simulation method helps us interpret that phenomenon.

Fig. 4 shows the hodographs of the wave run-up velocity at the two elevations along the armor layer. The vertical heights of the wave run-up and run-down are $R_{max}/h = 0.209$ and $R_{min}/h = -0.128$, respectively. The circles on the curves are time scale, which indicate the moments at every one eighth of the wave period. Arrows show the mean velocity vectors of the wave run-up velocity. The slope of armor layer of the breakwater is indicated with the dashed line. Above the elevation of the wave run-down, the hodographs are not closed. The direction of the mean flow at $z/h = 0.043$ is into the body of the permeable

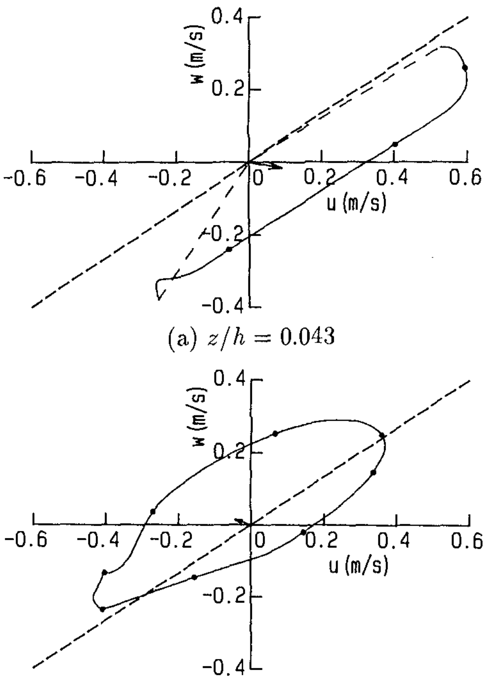

(a) $z/h = 0.043$

(b) $z/h = -0.245$

Fig. 4 Velocity hodograph

breakwater. The positive(upward) velocity perpendicular to the slope of the breakwater occurred below $z/h = -0.101$. Below the level of the wave run-down, $z/h < R_{min}/h = -0.128$, velocity hodographs are closed and make ellipses as shown in Fig. 4(b) $z/h = -0.245$, and the apsis of the velocity hodograph is parallel to the slope of the breakwater. Getting close to the bottom, the the apsis becomes parallel to the horizon and the ellipse of the wave run-up velocity becomes flat. The velocity hodograph is affected by the impermeable flat bed.

With the results of the numerical simulation, we discuss wave force action on armor units placed on the slope of the rubble-mound breakwater. Wave force acting on the armor units are estimated by using the Morison equation given by Eq. (15) with the velocity field near the armor layer.

$$\begin{aligned} F(x,z,t) &= F_D(x,z,t) + F_I(x,z,t) \\ &= \frac{1}{2}\rho C_D A u_s(x,z,t)\,|\,u_s(x,z,t)\,|+\rho C_M V \alpha_s(x,z,t) \end{aligned} \tag{15}$$

where F_D is the drag force and F_I the inertia force. The drag and inertia coefficients C_D, C_M of the single Tetrapod were obtained by Sakakiyama and Ka-

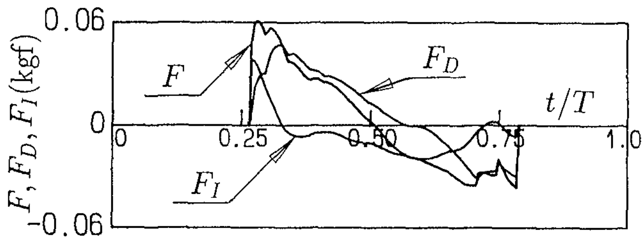

Fig. 5 Time histories of total wave force F, inertia force F_I and drag force F_D

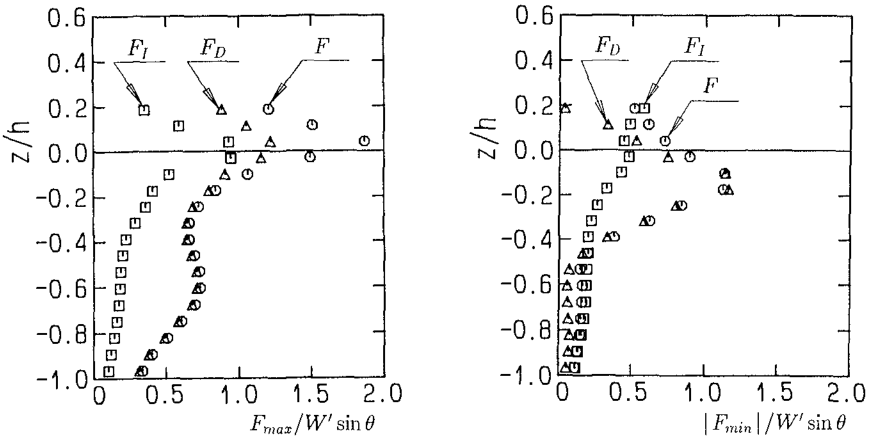

(a) During run-up (b) During run-down

Fig. 6 Vertical profile of wave force on armor units

jima(1990). They show the relationship between C_D, C_M and the Reynolds number with a parameter of KC number.

Fig. 5 shows the time histories of the wave forces. The drag and inertia coefficients are determined as $C_D = 1.0$ and $C_M = 1.0$, respectively referring to the results by Sakakiyama and Kajima(1990). The time history od the total wave force is very similar to the measured one obtained by Sakakiyama and Kajima(1990) excpet that the total wave force in Fig. 5 does not contain the buoyant weight of the armor unit. From the time history of the calculated wave force, the inertia force F_I works for a short time with a large peak behaving like a slamming force. The drag force F_D has longer duration than the inertia force. It is considered that the slamming force is not dangerous for the stability of the armor units because that force works into the body of the breakwater. However, the breakage of slender and fragile concrete armor units is due to this type of wave force causing the armor units to be rocking (Burcharth *et al.*,1991).

Fig. 6 shows the profiles of the wave force along the slope of the breakwater. The symbols indicate the peak values of the inertia, drag and total forces both

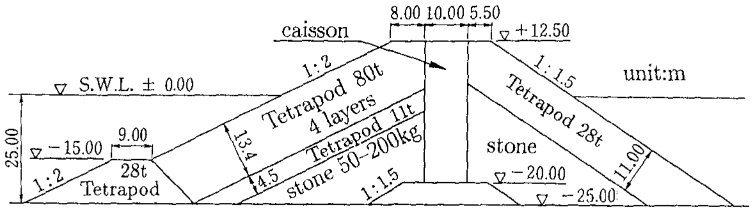

Fig. 7 Caisson breakwater($\lambda = 1/60$ and $1/15$)

Table 3 Experimental conditions for caisson breakwater in prototype

wave period	water depth	wave height H(m)	
T(s)	h(m)	λ =1/60	λ =1/15
15.5	25.0	1.08–17.64	1.08–16.92

during the wave run-up in Fig. 6(a) and during run-down in Fig. 6(b). The axis of abscissa indicates the ratio of the wave force to $W' \sin\theta$, where W' is the buoyant weight of an armor unit, θ the angle of breakwater slope. The ratio of the value of unity means the incipient condition of the armor unit when the friction force between armor units is neglected. The computational results shows that the profiles of the drag, inertia and total forces have the maximum values near the still water level during the wave run-up. During the wave-run down, the maximum value of the total wave force is found close to that of the drag force at $z/h \simeq -0.2$. It agrees with the fact that the armor units near the still water level are the most unstable as we have experienced in hydraulic experiments.

4. Caisson breakwater covered with armor units

4.1 Experiments

The experiments on a caisson breakwater covered with armor units were performed by using both a large wave flume(205m long, 6.0m deep and 3.4m wide) and a small one(78m long, 1.2m deep and 0.9m wide). The model scales were 1/15 and 1/60, respectively. Fig. 7 shows the prototype breakwater of which models were used in the scale model experiments. A narrow caisson is placed in the breakwater body to reduce transmitted waves. The core material consists of stones(W = 50kg to 200kg in prototype scale) of which porosity is estimated as ε =0.4. The weights of armor units are W = 80t in the armor layer at the windward side, W = 11t in the filter layer and W = 28t in the armor layer at the leeward side. The corresponding weights of the armor units in the 1/15-scale experiment were 20kg, 6.8kg and 10.0kg. Those used in the 1/60-scale experiment were 0.37kg, 0.054kg and 0.13kg. The *In Situ* porosity of armor and filter layers in the breakwater is ε = 0.50. The armor layer at the leeward side is placed to reduce multi-reflected waves in a harbor.

Table 3 shows the experimental conditions indicated in equivalent prototype

Table 4 Calculation condition for caisson breakwater

H(m)	T(s)	h(m)	L_I(m)	$\Delta x/L_I$	$\Delta z/h$	$\Delta t/T$	cal. region
9.00	11.6	25.0	191.24	1/114.7	1/15.0	1/200	$8.48 \times L$

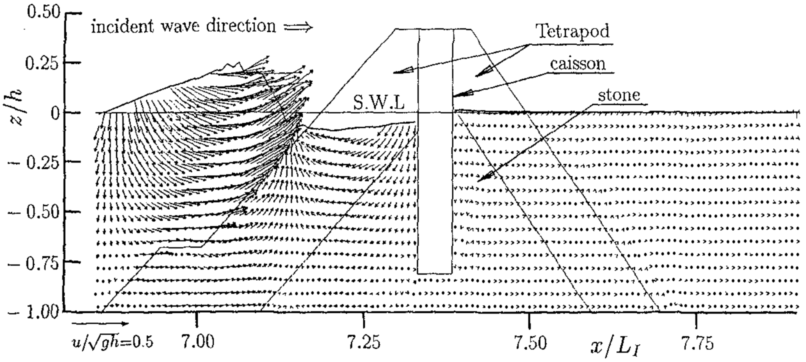

Fig. 8 Simulated result of wave transformation due to caisson breakwater

values. The reflection and transmission coefficients for various wave conditions (prototype wave conditions of incident wave height H = 1m to 17m, period $T = 15.5$s and water depth $h = 25.0$m) were obtained in the same way.

Measurements include also wave pressures on the seaward wall of the caisson covered with the permeable structures at 10 points in the large-scale experiments and at 6 points in the small-scale experiments.

4.2 Simulation of wave transformation

The computation was carried out under the wave conditions of the small scale-experiment such as the wave period $T = 1.5$s, the wave height at the breakwater $H = 0.15$m$(H/h = 0.36)$. Difference between the small- and large-scale conditions is the values of the inertia and drag coefficients which are functions of the Reynolds number and by which the scale effect is considered in the numerical simulation.

The computational condition is shown in Table 4 indicated in the prototype values. The horizontal distance of the calculation region was $8.48 \times L_I$, where L_I is the incident wave length at the uniform depth($h_I = 44.2$m) obtained from the nonlinear wave theory. The wave lengths are $L_I = 191.24$m at the uniform depth and $L = 161.16$m at the breakwater. The space increments are $\Delta x = \Delta z = 1.667$m($\Delta x/L_I = 1/114.7$ and $\Delta x/L = 1/96.7$ horizontally, $\Delta z/h = 1/15.0$ vertically). The time increment is $\Delta t = T/200$. It took about four hours with the main frame computer HITAC 680H to calculate 4000 time steps(20 cycles $\times$ 200 steps per wave period) to gain the steady state wave motion near the caisson breakwater.

The reflection and transmission coefficients obtained in the calculation for the

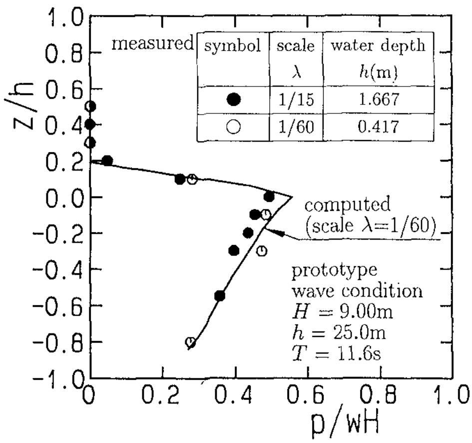

Fig. 9 Comparison of wave pressure between calculation and experiment

small-scale model are $K_R = 0.18$ and $K_T = 0.010$. The corresponding small-scale experimental results are $K_R = 0.21$ and $K_T = 0.015$, respectively. The computation which reproduced the experiment best gives $C_M = 1.2$ and $C_D = 0.9$.

Fig. 8 shows the computed wave velocity field and the surface profile for the small-scale model when the wave runs up on the slope at the windward side of the permeable breakwater. The wave surface profile is deformed on the slope of the armor layer resulting in a steeper surface at the leeward side than that at the windward. Velocity of the wave front just outside the armor layer is increased according to the wave deformation. The velocity inside the armor layer is small and discharge also smaller than that outside the armor layer. The difference of the velocity between inside and outside the armor layer is large and the flow is concentrating to the surface of the armor layer. It is concluded that the velocity field is reasonably simulated as a whole.

The inertia and drag coefficients C_M and C_D in the computation were estimated so that the reflection and transmission coefficients obtained by the experiment might agree well with the those obtained by the computation, respectively. In order to verify the present method, it is necessary to compare other values between the experiment and the computation. Thus a wave-induced pore pressure is compared between the computed and measured results as shown in Fig. 9, where w is the specific weight of fluid. It is found that the quantitative agreement of the computed pressure profile with the measured one is very good for the small-scale experiment. The large-scale experimental result is also shown in Fig. 9. The scale effect on the pressure will be discussed in the following subsection.

4.3 Scale effect of wave transformation and pressure

Fig. 10 shows the results of the reflection and transmission coefficients obtained through the large- and small-model scale experiments. The factor of the model scale according to the Froude law is 4(the large-model scale is 1/15 and the small

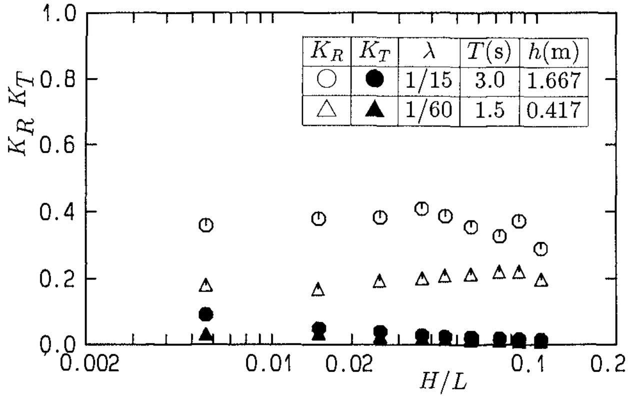

K_R	K_T	λ	T(s)	h(m)
○	●	1/15	3.0	1.667
△	▲	1/60	1.5	0.417

Fig. 10 Scale effect of reflection and transmission coefficients

one 1/60). It is found that the reflection coefficients of the large-scale experiments are larger than the small ones. The transmission coefficients of the large-scale experiments are larger than small-scale one, although the difference is very small. Consequently, the energy dissipation rate of the large-scale experiments is less than that of the small-scale ones.

The tendency of the scale effect on the wave pressure is opposite to that on the wave reflection as shown in Fig. 9 on the pressure profiles comparing between the experimental results with the large- and small-scale models. That is, the wave pressures in the small-scale hydraulic experiments are larger than those in the large-scale one.

It is concluded from the results of the scale effects on the wave reflection and the wave pressure that the wave pressure is small when the wave reflection is large. It is very natural and explained as follows: When the reflection coefficient is large, a small amount of wave penetrates in a permeable structure and onto the caisson. As the result, the wave pressure becomes small.

The scale effects on the wave reflection and wave pressure mentioned above is explained with the following numerical experiments. Fig. 11 shows the effect of the inertia coefficient on the wave pressure, when the drag coefficient is constant as C_D=0.9. The computation are performed by varying the inertia coefficient C_M with 1.2, 1.5 and 1.7. As the inertia coefficient C_M increases the wave pressure decreases. On the other hand, the reflection coefficient increases as the inertia coefficient C_M increases. The transmission coefficient decreases very slightly. The reflection and transmission coefficients are less sensitive to the change of the inertia coefficient C_M than the wave pressure.

As the inertial resistance described by the factor $\lambda_v = \gamma_v + (1 - \gamma_v)C_M$ defined as Eq. (4) increases, the wave reflection from the armor and filter layers increases. Consequently, the less part of wave transmits in the permeable structure and the wave pressure decreases. As the Reynolds number increases under the condition that KC number is constant, the inertia coefficient increases according to the Froude law for scaling.

Fig. 12 shows the effect of drag coefficient on the wave pressure, while the inertia coefficient is constant as $C_M = 1.5$. The drag coefficient C_D is selected as $C_D = 0.3, 0.6$ and 0.9. As the drag coefficient increases, the wave pressure decreases. It is caused by an increase of the wave energy dissipation in the permeable structure.

As explained above, both the drag and inertia coefficients influence the scale effect on the wave reflection, transmission and also the pressure. These scale effects are reflected to the numerical model through C_M and C_D which are functions of the Reynolds number.

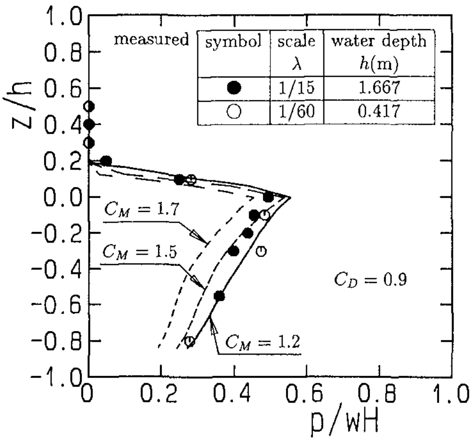

Fig. 11 Wave pressure depending on inertia coefficient($C_D = 0.9$)

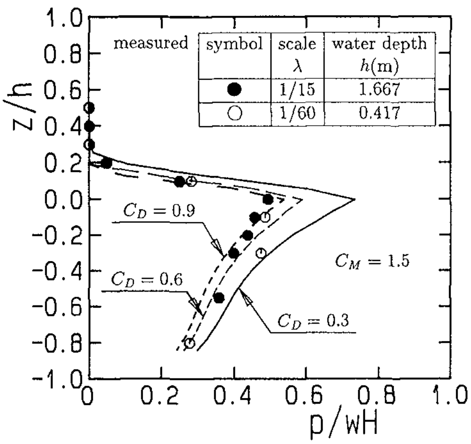

Fig. 12 Wave pressure depending on drag coefficient($C_M = 1.5$)

5. Conclusions

A fully nonlinear numerical model has been developed to simulate the wave motion near and in a permeable breakwater. The simulated results were compared with hydraulic experimental ones using two types of permeable breakwaters, a rubble-mound breakwater and a caisson breakwater covered with armor units. The present model can reproduce the wave reflection and transmission, and also the pressure on the caisson. Wave profiles and velocity fields near and in the permeable breakwaters were realistically simulated. Wave force acting on armor units was estimated by Morison equation with the computed velocity. The maximum wave force was found near the still water level during wave run-up.

The scale effects on the wave reflection, transmission and wave-induced pore pressure were demonstrated by the hydraulic experiments. Computation interprets these scale effects. As model scale increases the drag coefficient decreases and the inertia coefficient increases. As the result, the wave energy dissipation due to the drag force decreases while the wave reflection increases due to the inertial resistance. Consequently, the scale effect on the wave-induced pore pressure is canceled by two opposite effects of fluid resistance.

The drag and inertia coefficients were determined so that the reflection and transmission coefficients of the experiment fit with those of the computation, respectively. A fundamental experiment, an oscillation flow test using U-tube tank, for instance will be required to estimate the inertia and drag coefficients.

REFERENCES

Ohyama,T and K. Nadaoka(1991): Development of a numerical wave tank for analysis of nonlinear and irregular wave field, *Fluid Dynamics Res.*, 8, pp.231–251.

Burcharth,H.F., G.L.Howell and Z.Liu(1991): On the determination of concrete armour unit stresses including specific results related to Dolosse, *Coastal Engineering*, 15, pp.107–165.

Chan,R.K.C. and R.L.Street(1970): A computer study of finite-amplitude water waves, *J. Computational Physics*, 6, pp.68-94.

Hölscher, P., de Groot, M. P. and J.W. van der Meer(1989): Simulation of internal water movement in breakwater, *Modelling Soil-Water-Structure Interaction*, pp.427–433.

Wurjanto,A. and N. Kobayashi(1992): Irregular wave prediction and run-up on permeable slope, *J. Waterway, port, coastal and ocean Engineering*, ASCE, (submitted).

Sakakiyama,T. and R.Kajima(1990): Scale effect of wave force on armor units, *Proc. 22nd Coastal Engineering Conf.*, ASCE, Vol.2, pp.1716–1729.

Sakakiyama,T(1991): Nonlinear-wave interaction with permeable breakwaters, *Extended Abstract of 4th Int. Conf. Computing in Civil and Building Engineering.*

Goda, Y.(1985): Random seas and design of maritime structures, University of Tokyo Press, 323p.